PHYSICAL REVIEW B **83**, 184401 (2011)

Lattice symmetries and regular magnetic orders in classical frustrated antiferromagnets

L. Messio,[1] C. Lhuillier,[2] and G. Misguich[3]

[1]*Institute of Theoretical Physics, Ecole Polytechnique Fédérale de Lausanne, CH-1015 Lausanne, Switzerland*

[2]*Laboratoire de Physique Théorique de la Matière Condensée, UMR 7600 CNRS, Université Pierre et Marie Curie, Paris VI, 75252 Paris Cedex 05, France*

[3]*Institut de Physique Théorique, CNRS, URA 2306, CEA, IPhT, 91191 Gif-sur-Yvette, France*

(Received 6 January 2011; revised manuscript received 8 March 2011; published 6 May 2011)

We consider some classical and frustrated lattice spin models with global O(3) spin symmetry. No general analytical method to find a ground state exists when the spin dependence of the Hamiltonian is more than quadratic (i.e., beyond the Heisenberg model) and/or when the lattice has more than one site per unit cell. To deal with these cases, we introduce a family of variational spin configurations, dubbed "regular magnetic orders" (RMO's), which respect all the lattice symmetries *modulo global* $O(3)$ *spin transformations* (rotations and/or spin flips). The construction of these states is made explicit through a group-theoretical approach, and all the RMO's on the square, triangular, honeycomb, and kagome lattices are listed. Their equal-time structure factors and powder averages are shown for comparison with experiments. Well known Néel states with one, two, or three sublattices on various lattices are RMO's, but the RMO's also encompass exotic nonplanar states with cubic, tetrahedral, or cuboctahedral geometry of the $T = 0$ order parameter. Regardless of the details of the Hamiltonian (with the same symmetry group), a large fraction of these RMO's are energetically stationary with respect to small deviations of the spins. In fact, these RMO's appear as exact ground states in large domains of parameter space of simple models that we have considered. As examples, we display the variational phase diagrams of the J_1-J_2-J_3 Heisenberg model on all the previous lattices as well as that of the J_1-J_2-K ring-exchange model on square and triangular lattices.

DOI: 10.1103/PhysRevB.83.184401 PACS number(s): 75.10.Hk, 75.40.Cx

I. INTRODUCTION

Finding the ground state (GS) of an antiferromagnetic *quantum* spin model is a notoriously difficult problem. Moreover, even *classical* spin models at zero temperature can be nontrivial to solve, unless one carries some extensive numerical investigation. In particular, there is no general method to determine the lowest-energy configurations for a simple Heisenberg O(3) model of the type

$$E = \sum_{i,j} J(|\mathbf{x}_i - \mathbf{x}_j|)\mathbf{S}_i \cdot \mathbf{S}_j \tag{1}$$

if the lattice sites $\{\mathbf{x}_i\}$ do *not* form a Bravais lattice. Only when there is a single site per unit cell (Bravais lattice) can one easily construct some GS[1] (see Sec. VI B).

Another situation in which the classical energy minimization is not simple is that of multiple-spin interactions, where the energy is not quadratic in the spin components. Finding the GS in the presence of interactions of the type $(\mathbf{S}_i \cdot \mathbf{S}_j)(\mathbf{S}_k \cdot \mathbf{S}_l)$ can be difficult and, in general, has to be done numerically even on Bravais lattices. Such terms arise in the classical limit of ring-exchange interactions. For instance, the—apparently simple—classical model with Heisenberg interactions competing with four-spin ring exchange on the triangular lattice is not completely solved.[2]

In this study, we introduce and construct a family of spin configurations, dubbed "regular magnetic orders" (RMO's). These configurations are those that respect all the symmetries of a given lattice *modulo global spin transformations* (rotations and/or spin flips). This property is obeyed by most usual Néel states. For instance, the two- (three-) sublattice Néel state on the square (triangular) lattice, that is the GS of the antiferromagnetic first-neighbor Hamiltonian, respects the lattice symmetries: each symmetry operation can be "compensated" by the appropriate global spin rotation of angle 0 or π $(0, \pm 2\pi/3)$.

By definition, the set of RMO's only depends on the symmetries of the model—the lattice symmetries and the spin symmetries—and therefore does not depend on the strength of the different interactions $[J(|\mathbf{x}|)$ in the example of Eq. (1)]. These states comprise well-known structures, such as the two- and three-sublattice Néel states mentioned above, but also some new states, such as nonplanar structures on the kagome lattice, that will be discussed in Sec. IV A.

The reason why these states are interesting for the study of frustrated antiferromagnets is that they are good "variational candidates" to be the ground state of many specific models. In fact, rather surprisingly, we found that these states (together with spiral states) exhaust all the GS's in a large range of parameters of the frustrated spin models we have investigated. For instance, in the case of a Heisenberg model on the kagome lattice (studied in Sec. VI C) with competing interactions between first, second, and third neighbors, some nonplanar spin structures (based on a cuboctahedron) turn out to be stable phases. In other words, the set of RMO's and spiral states forms a good starting point to determine the phase diagram of a classical O(3) model, without having to resort to lengthy numerical minimizations: once all the RMO's have been constructed for given lattice and spin symmetries (using a simple group-theoretic construction, as explained in Sec. III), one can directly compare their energies for a given microscopic Hamiltonian. In several cases, we even observed that one of the RMO's reaches an exact energy lower bound, therefore proving that it is one (maybe not unique) GS of the model.

These states may also be used when analyzing experimental data on magnetic compounds where the lattice structure is known, but where the values (and range) of the magnetic interactions are not. In such a case, the (equal-time) magnetic correlations—measured by neutron scattering—can be directly compared to those of the RMO's. If these correlations match those of one RMO, this may be used, in turn, to get some information about the couplings. With this application in mind, we provide the magnetic structure factors of all the RMO's we construct and powder averages of some of them (see Appendix B).

The organization of the paper is as follows: In Sec. II, we present the definition of an RMO, a state that weakly breaks the lattice symmetries and all the notations needed for the group-theoretical approach. In Sec. III A, we explain the algebraic structure of the group of joint space and spin transformations that leave a regular spin configuration invariant (algebraic symmetry group) and describe it for the triangular lattice (detailed calculations are given in Appendix A). We then explain how to construct RMO's in Sec. III B. This approach is algebraically very similar to Wen's construction of symmetric spin liquids,[3] but there are also strong differences in the invariance requirements: whereas the symmetric spin liquids do not break lattice symmetries (they are "liquids"), our RMO's indeed break lattice symmetries but in a "weak" way (see Appendix C). These subsections are self-contained, but can be skipped by readers interested essentially in the results. In Sec. III C, we construct all the RMO's on the triangular lattice. In Secs. IV A and IV B, we list the RMO's on the kagome and honeycomb lattices (which have the same algebraic symmetry group as the triangular lattice), and with a minimum of algebra we present the RMO's on the square lattice (Sec. IV C). We then show that spiral states can be seen in this picture as RMO's with a lattice symmetry group reduced to the translation group (Sec. IV D). In Sec. V, we discuss geometrical properties of RMO's and the relationship between RMO's and representations of the lattice symmetry group. This section can be skipped by readers more interested in physics than in geometry. In Sec. VI, we study the energetics of these RMO's and therefore their interest for the variational description of the $T = 0$ phase diagrams of frustrated spin models. We first show in Sec. VI A that all RMO's that do not belong to a continuous family are energetically stationary with respect to small spin deviations and thus good GS candidates for a large family of Hamiltonians. After having given a lower bound on the energy of Heisenberg models (Sec. VI B), we then show that over a large range of coupling constants, the RMO's are indeed exact GS's of the J_1-J_2-J_3 model on the honeycomb and kagome lattices (Sec. VI C). We then display in Sec. VI D a variational phase diagram of the J_1-J_2-K model on square and triangular lattices. In Sec. VI E, we discuss finite-temperature phase transitions: the nonplanar states are chiral and should give rise to a $T \neq 0$ phase transition. Section VII contains our conclusion.

The calculation of the algebraic symmetry groups on the triangular lattice is detailed in Appendix A. Powder averages of the structure factors of the RMO's on triangular and kagome lattices are displayed in Appendix B. Analogies and differences between the present analysis and Wen's analysis of quantum spin models are explained in Appendix C.

II. NOTATIONS AND DEFINITIONS

We will mostly concentrate on Heisenberg-spin models where on each lattice site i, the spin $\mathbf{S}_i$ is a three-component unit vector. But the concept of an RMO can be easily extended to the general situation in which $\mathbf{S}_i$ belongs to another manifold $\mathcal{A}$ (such as for nematic or quadrupolar order parameters that are encountered in some quantum systems).

We note by S_S the group of the "global spin symmetries" of the Hamiltonian. In the general framework, an element of S_S is a mapping of $\mathcal{A}$ onto itself, which does not change the energy of the spin configurations. For a Heisenberg model without applied magnetic field, S_S is simply (isomorphic to) the orthogonal group O(3). In a similar way, we note by S_L the lattice symmetry group of the Hamiltonian. An element of S_L acts on spin configurations by mapping the lattice L onto itself and is the identity in the spin space $\mathcal{A}$.

In this paper, we will restrict ourselves to the (rather common) situation in which the full symmetry group S_H of the model is the direct product $S_S \times S_L$. (A case in which $S_H \neq S_S \times S_L$ is the antiferromagnetic square lattice with a site-dependent magnetic field taking two opposite values on each sublattice. The spin inversion $\mathbf{S}_i \to -\mathbf{S}_i$ is not in S_S, the translation by one lattice spacing is not in S_L, but the composition of both is in S_H. The theory developed in this paper can, however, be used in this case by replacing S_L by S_H/S_S.)

Let $\mathcal{G}$ be the set of all the applications from the lattice symmetry group S_L to the spin symmetry group S_S. An element G of $\mathcal{G}$ associates a spin symmetry G_X to each lattice symmetry X:

$$\begin{aligned} G : S_L &\to S_S, \\ X &\mapsto G_X. \end{aligned} \tag{2}$$

We now concentrate on a fixed spin configuration c. H_c denotes its stabilizer, that is, the subgroup of S_H whose elements do not modify c. Its spin symmetry group H_c^S is the group of unbroken spin symmetries: $H_c^S = S_S \cap H_c$.

We introduce two definitions:

(i) A mapping $G \in \mathcal{G}$ is said to be compatible with a spin configuration c if the composition of an element of S_L with its image by G leaves c unchanged:

$$\forall X \in S_L, \quad G_X X \in H_c. \tag{3}$$

(ii) A configuration c is said to be regular if any lattice symmetry $X \in S_L$ can be "compensated" by an appropriate spin symmetry $G_X \in S_S$, which means $G_X X|c\rangle = |c\rangle$ (that is, $G_X X \in H_c$). In other words, c is an RMO if there exists a mapping $G \in \mathcal{G}$ such that G and c are compatible.

In an RMO, the observables that are invariant under S_S are therefore invariant under all lattice symmetries. These definitions are summarized in Fig. 1.

The simplest RMO's are those that are already invariant under lattice symmetries (i.e., $S_L \subset H_c$), without the need to perform any spin symmetry. This is the case of a ferromagnetic (F) configuration, with all spins oriented in the same way. But less trivial possibilities exist, such as the classical GS of the antiferromagnetic (AF) first-neighbor Heisenberg interaction on the square lattice. This GS possesses two sublattices with opposite spin orientations. Each lattice symmetry X either conserves the spin orientations or reverses them, so we can

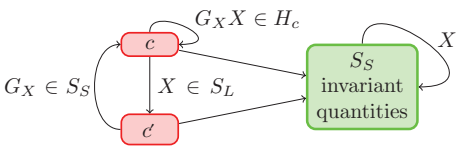

FIG. 1. (Color online) A lattice symmetry $X \in S_L$ acts on a spin configuration c to give a new configuration $c' = Xc$. If c is regular, there is a spin symmetry $G_X \in S_S$ such that one gets back the initial state: $G_X c' = c$.

choose as G_X either the identity or the spin inversion $\mathbf{S}_i \to -\mathbf{S}_i$.

If the subgroup $H_c^S = S_S \cap H_c$ of unbroken spin symmetries contains more than the identity, there are several elements of $\mathcal{G}$ compatible with c. For each X, there are as many G_X as elements in H_c^S. In the previous example of the GS of the AF square lattice, H_c^S is the set of spin transformations that preserve the two opposite spin orientations: this group is isomorph to O(2). Beginning with a compatible G, each G_X can be composed with an element of H_c^S to give another compatible element of $\mathcal{G}$.

To summarize, RMO's are not restricted to states strictly respecting the lattice symmetries, but to states that in some way *weakly* respect them. We will now explain how to construct *all* the regular spin configurations on a given lattice.

III. CONSTRUCTION OF RMO's

To construct the RMO's, we proceed in two steps. *In the first step, we fix a given unbroken spin symmetry group* H_c^S, and consider the algebraic constraints that the lattice symmetry group S_L imposes on a mapping $G \in \mathcal{G}$, assuming that some (so far unknown) spin configuration c is compatible with G. These constraints lead to a selection of a subset $\mathcal{G}^A$ of $\mathcal{G}$, composed of the mappings G that are compatible with the lattice symmetries. For an element G of $\mathcal{G}^A$, the group

$$H^G = \{G_X X, X \in S_L\} \times H_c^S \tag{4}$$

is dubbed the *algebraic symmetry group* associated with G.

When $H_c^S = \{I\}$, the algebraic symmetry groups are an extension of the magnetic space groups,[4] which are themselves an extension of the crystallographic space groups. To go from crystallographic to magnetic space groups, the time-reversal transformation or the identity is combined to each of the lattice transformations. Points of the lattice have black or white points. To go from crystallographic to algebraic symmetry groups, a spin transformation is combined to each of the lattice transformations. Now points of the lattice carry elements of S_S.

In three dimensions (3D), there are 230 crystallographic space groups. In 2D, they reduce to the 17 wallpaper groups. In the following sections, we are going to derive all the algebraic symmetry groups derived from two of the wallpaper groups, denoted *p6m* (triangular Bravais lattice of Fig. 2) and *p4m* (square Bravais lattice of Fig. 2) in the Hermann-Mauguin notations. These are the simplest cases in 2D because they are the most constrained, thus they have the fewest groups. But we could derive the algebraic symmetry group of any of the two- or three-dimensional crystallographic space groups by the same procedure as in these examples.

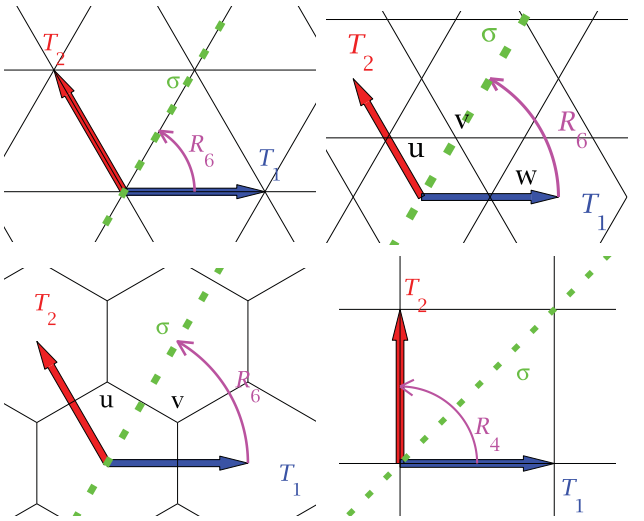

FIG. 2. (Color online) Generators of the lattice symmetries group S_L for the triangular, kagome, honeycomb, and square lattices. For the first three lattices: the two translations T_1 and T_2 (along the two basis vectors $\mathbf{T}_1$ and $\mathbf{T}_2$), the reflection σ and the rotation R_6 of angle $\pi/3$. For the square lattice, generators of S_L are T_1, T_2, σ, and the rotation R_4 of angle $\pi/2$.

In the second step of the RMO construction, one determines the configurations (if any) that are compatible with a given algebraic symmetry group.

A. Algebraic symmetry groups

We fix the spin symmetry group H_c^S (to be exhaustive, we will consecutively consider each possible H_c^S). Let X, Y, and Z be three elements of S_L such that $XY = Z$. We will see that this algebraic relation imposes some constraints on the mappings G that are compatible with a spin configuration. Indeed, we assume that there exists a configuration c compatible with G. Then, $G_Z Z$ and $G_X X G_Y Y$ are in H_c. This implies that $G_X X G_Y Y Z^{-1} G_Z^{-1}$ is also in H_c. Elements of S_L and S_S commute, so we have $G_X X G_Y Y Z^{-1} G_Z^{-1} = G_X G_Y G_Z^{-1}$, which is a pure spin transformation. We deduce that

$$\forall X, Y \in S_L, \quad G_X G_Y G_{(XY)}^{-1} \in H_c^S. \tag{5}$$

If the above constraint is not satisfied, G must be excluded from the set $\mathcal{G}^A$ of the algebraically compatible mappings.

Now we illustrate these general considerations using the following example: L is an infinite triangular lattice and the spin space $\mathcal{A}$ is the two-dimensional sphere $\mathcal{S}_2$ (Heisenberg spins). S_L is generated by two translations T_1 and T_2 along vectors $\mathbf{T}_1$ and $\mathbf{T}_2$, a reflection σ, and a rotation R_6 of angle $\pi/3$, described in Fig. 2 and defined in the $(\mathbf{T}_1, \mathbf{T}_2)$ basis as

$$T_1 : (r_1, r_2) \mapsto (r_1 + 1, r_2), \tag{6a}$$
$$T_2 : (r_1, r_2) \mapsto (r_1, r_2 + 1), \tag{6b}$$
$$\sigma : (r_1, r_2) \mapsto (r_2, r_1), \tag{6c}$$
$$R_6 : (r_1, r_2) \mapsto (r_1 - r_2, r_1). \tag{6d}$$

The spin symmetry group S_S is chosen to be O(3) (as for a Heisenberg model). In such a system, the unbroken symmetry group H_c^S is either isomorph to $\{I\}$, $\mathbb{Z}_2$, or O(2), depending

on the orientations of the spins (noncoplanar, coplanar, or collinear, respectively). The nonplanar case, $H_c^S = \{I\}$, is the most interesting case and we choose it for this example. The two other cases can be treated by reducing $\mathcal{A}$ to the circle $\mathcal{S}_1$ or $\mathcal{S}_0 = \{1, -1\}$ (XY or Ising spins) and S_S to O(2) or O(1) to have $H_c^S = \{I\}$, which simplifies the calculations considerably.

We assume that a mapping G belongs to $\mathcal{G}^A$ (algebraically compatible). As $H_c^S = \{I\}$, Eq. (5) allows us to construct the full mapping G simply from the images of the generators of the lattice symmetry group S_L. As several combinations of generators can produce the same element of S_L, the images by G of the S_L generators must satisfy some algebraic relations. These relations were needed in a similar algebraic study in Ref. 5 and consist in all the relations necessary to put each product of generators in the form $\sigma^s R_6^r T_1^{t_1} T_2^{t_2}$, where $s = 0,1$, $r = 0,1,\ldots,5$, and $t_1, t_2 \in \mathbb{Z}$. These relations are

$$T_1 T_2 = T_2 T_1, \tag{7a}$$
$$T_1 R_6 T_2 = R_6, \tag{7b}$$
$$R_6 T_1 T_2 = T_2 R_6, \tag{7c}$$
$$T_1 \sigma = \sigma T_2, \tag{7d}$$
$$R_6^6 = I, \tag{7e}$$
$$\sigma^2 = I, \tag{7f}$$
$$R_6 \sigma R_6 = \sigma. \tag{7g}$$

From these equations and from Eq. (5), we get

$$G_{T_1} G_{T_2} = G_{T_2} G_{T_1}, \tag{8a}$$
$$G_{T_1} G_{R_6} G_{T_2} = G_{R_6}, \tag{8b}$$
$$G_{R_6} G_{T_1} G_{T_2} = G_{T_2} G_{R_6}, \tag{8c}$$
$$G_{T_1} G_\sigma = G_\sigma G_{T_2}, \tag{8d}$$
$$G_{R_6}^6 = I, \tag{8e}$$
$$G_{\sigma^2} = I, \tag{8f}$$
$$G_{R_6} G_\sigma G_{R_6} = G_\sigma. \tag{8g}$$

The details of the calculations are given in Appendix A. The solutions can be divided in three families:

$$G_{T_1} = G_{T_2} = I, \tag{9a}$$
$$\theta_{T_1} = \theta_{T_2} = \pi \text{ and } \mathbf{n}_{T_1} \perp \mathbf{n}_{T_2}, \tag{9b}$$
$$G_{T_1} = G_{T_2} \neq I, \tag{9c}$$

where each element G_X is characterized by its determinant $\varepsilon_X = \pm 1$ (not appearing here) and by a rotation $R_{\mathbf{n}_X \theta_X}$ of axis $\mathbf{n}_X$ and of angle $\theta_X \in [0,\pi]$ such that $G_X = \varepsilon_X R_{\mathbf{n}_X \theta_X}$. Up to a global similarity relation $[G_X \to M G_X M^{-1}, M \in \mathrm{SO}(3)]$, we obtain 28 solutions of the system of Eqs. (8) in the case of Eq. (9a), four for Eq. (9b), and eight for Eq. (9c). The 40 solutions are listed below:

$$G_{T_1} = G_{T_2} = I, \quad G_\sigma = \varepsilon_\sigma I, \quad G_{R_6} = \varepsilon_R I, \tag{10a}$$
$$G_{T_1} = G_{T_2} = I, \quad G_\sigma = \varepsilon_\sigma I, \quad G_{R_6} = \varepsilon_R R_{\mathbf{z}\pi}, \tag{10b}$$
$$G_{T_1} = G_{T_2} = I, \quad G_\sigma = \varepsilon_\sigma R_{\mathbf{z}\pi}, \quad G_{R_6} = \varepsilon_R I, \tag{10c}$$
$$G_{T_1} = G_{T_2} = I, \quad G_\sigma = \varepsilon_\sigma R_{\mathbf{z}\pi}, \quad G_{R_6} = \varepsilon_R R_{\mathbf{z}\pi}, \tag{10d}$$
$$G_{T_1} = G_{T_2} = I, \quad G_\sigma = \varepsilon_\sigma R_{\mathbf{z}\pi}, \quad G_{R_6} = \varepsilon_R R_{\mathbf{x}\pi}, \tag{10e}$$
$$G_{T_1} = G_{T_2} = I, G_\sigma = \varepsilon_\sigma R_{\mathbf{z}\pi}, G_{R_6} = \varepsilon_R R_{\mathbf{x}\theta}, \tag{10f}$$
$$G_{T_1} = R_{\mathbf{x}\pi}, G_{T_2} = R_{\mathbf{y}\pi}, \quad G_\sigma = -\varepsilon_\sigma \begin{pmatrix} 0 & 1 & 0 \\ 1 & 0 & 0 \\ 0 & 0 & 1 \end{pmatrix}, \quad G_{R_6} = \varepsilon_R \begin{pmatrix} 0 & 1 & 0 \\ 0 & 0 & 1 \\ 1 & 0 & 0 \end{pmatrix}, \tag{10g}$$
$$G_{T_1} = G_{T_2} = R_{\mathbf{z}\frac{2\pi}{3}}, G_\sigma = \varepsilon_\sigma I, G_{R_6} = \varepsilon_R R_{\mathbf{x}\pi}, \tag{10h}$$
$$G_{T_1} = G_{T_2} = R_{\mathbf{z}\frac{2\pi}{3}}, G_\sigma = \varepsilon_\sigma R_{\mathbf{z}\pi}, G_{R_6} = \varepsilon_R R_{\mathbf{x}\pi}, \tag{10i}$$

where $\mathbf{x} \perp \mathbf{z}$, $\varepsilon_\sigma, \varepsilon_R = \pm 1$, and $\theta \in \{\frac{\pi}{3}, \frac{2\pi}{3}\}$. Each line corresponds to four solutions, except for Eq. (10f) with eight solutions. We stress that the algebraic symmetry groups depend on S_S, H_c^S, and on the algebraic properties of S_L, but not directly on the lattice L. In particular, different lattices can have the same algebraic symmetry groups. The results, Eqs. (10), are exactly the same on a honeycomb or a kagome lattice with symmetries of Fig. 2 because the algebraic equations (7) stay the same.

B. Compatible states

The second step consists in taking each element of $\mathcal{G}^A$ and finding all the compatible states. This last step is fully lattice-dependent.

To construct an RMO compatible with some mapping $G \in \mathcal{G}^A$, one first chooses the direction of the spin on a site i. Then, by applying all the transformations of S_L, we deduce the spin directions on the other sites. A constraint appears when two different transformations X and Y lead to the same site $X(i) = Y(i)$. The image spins have to be the same: $G_X(\mathbf{S}_i) = G_Y(\mathbf{S}_i)$. It can either give a constraint on the direction of $\mathbf{S}_i$ or indicate that no G-compatible state exists.

To find these constraints, we divide the lattice sites in orbits under the action of S_L (if all the sites are equivalent, there is a single orbit). In each orbit, we choose a site i. Each nontrivial transformation X that does not displace i gives a constraint: $G_X(\mathbf{S}_i) = \mathbf{S}_i$. For each $G \in \mathcal{G}^A$, the associated RMO's are obtained by choosing a site in each orbit, a spin direction respecting the site constraints, and then propagating the spin directions through the lattice using the symmetries in S_L.

C. Example of RMO construction: The triangular lattice

Let us apply this method to the example of the triangular lattice. There is a single orbit, and the transformations that leave the site of coordinates (0,0) in the $(\mathbf{T}_1, \mathbf{T}_2)$ basis invariant (see Fig. 2) are generated by σ and R_6, giving the two constraints $G_\sigma(\mathbf{S}(0,0)) = G_{R_6}(\mathbf{S}(0,0)) = \mathbf{S}(0,0)$.

The mapping of Eq. (10a) has compatible states only for $\varepsilon_R = \varepsilon_\sigma = 1$. They are ferromagnetic (F) states, as shown in Fig. 3(a). Since $G_{T_{1-2}} = I$ for Eqs. (10b)–(10f), no new RMO's can be compatible with any of them.

The mapping of Eq. (10g) has compatible states only for $\varepsilon_R = 1$ and $\varepsilon_\sigma = -1$. Then $\mathbf{S}(0,0) = \pm(1,1,1)/\sqrt{3}$ and the state is the tetrahedral state depicted in Fig. 3(b), where the spins of four sublattices point toward the corners of a tetrahedron. The sign of $\mathbf{S}(0,0)$ determines the chirality of the configuration.

The next RMO is the coplanar state of Fig. 3(c), which is compatible with Eq. (10i) for $\varepsilon_R = \varepsilon_\sigma = 1$ and $\mathbf{S}(0,0) = \pm(1,0,0)$. The three sublattices are coplanar with relative angles of 120°. This state is not chiral because the configurations

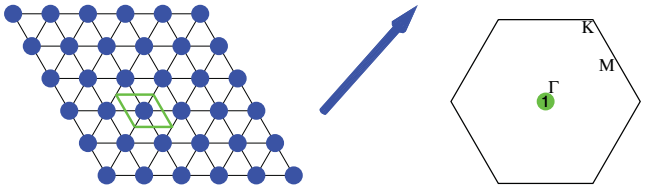

(a) Ferromagnetic (F) state. $E = 6J_1 + 6J_2 + 6J_3 + 42K.$

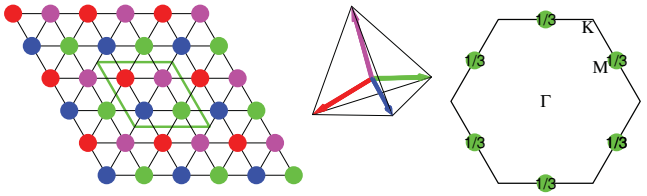

(b) Tetrahedral state. $E = -2J_1 - 2J_2 + 6J_3 - 34K/3.$

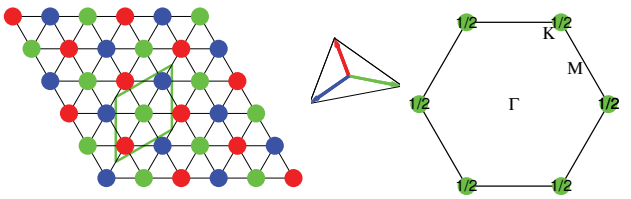

(c) Coplanar state. $E = -3J_1 + 6J_2 - 3J_3 - 3K.$

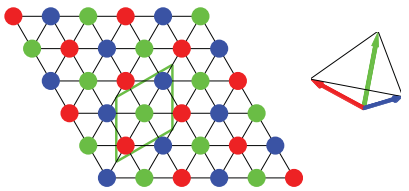

(d) F umbrella states.

FIG. 3. (Color online) Regular magnetic orders on the triangular lattice. The sublattice arrangements (labeled by colors) and the spin directions on each sublattice are displayed in the left and center columns. A spin unit cell is surrounded with green lines. The positions and weights of the Bragg peaks in the hexagonal Brillouin zone of the lattice are in the right column. The energy per site of each structure is given as a function of the parameters of the models described in Sec. VI.

obtained with the two possible $\mathbf{S}(0,0)$ are related by a global spin rotation in SO(3).

A continuum of *umbrella* states are compatible with Eq. (10i) with $\varepsilon_\sigma = 1$ and $\varepsilon_R = -1$. They are depicted in Fig. 3(d), where the sublattices are the same as those for the coplanar states but the relative angles between the spin orientations are all identical and $\leqslant 120^\circ$. This family interpolates between the F and the coplanar states.

We started by choosing $H_c^S = \{I\}$, but states with $H_c^S = \mathbf{Z}_2$ (for the coplanar state) or O(2) (for the F state) have been obtained anyway. One can check that choosing another H_c^S would not give any new RMO. All the RMO's are thus those gathered in Fig. 3.

The Bragg peaks of these states are displayed in the hexagonal Brillouin zone in the right column of Fig. 3 and their powder-averaged structure factors in Appendix B together with the formulas for these quantities.

IV. REGULAR MAGNETIC ORDERS FOR HEISENBERG SPINS ON SEVERAL SIMPLE LATTICES

In the following, we enumerate the RMO's on the kagome and honeycomb lattices, two lattices that have a symmetry group S_L isomorphic to that of the triangular lattice. To be complete, we also present the RMO's on the square lattice and discuss the spiral states that may be seen as RMO's when S_L reduces to the translation group.

A. Kagome lattice

The symmetry group S_L of the kagome lattice is isomorphic to that of the triangular lattice, thus the algebraic solutions Eqs. (10) remain valid. Carrying out the approach of Sec. III B for this new lattice, one obtains all the RMO's on the kagome lattice. They are displayed in Fig. 4 together with the positions and weights of the Bragg peaks and are listed below. The equal-time structure factor is depicted in the extended Brillouin zone (EBZ), drawn with thin lines in Fig. 4: the kagome lattice has three sites per unit cell of the underlying triangular lattice and the EBZ has a surface four times larger than the BZ of the underlying triangular Bravais lattice, drawn with dark lines. Powder-averaged structure factors of the RMO's are given in Appendix B.

One RMO is collinear [$H_c^S = \mathrm{O}(2)$]:

(i) The ferromagnetic (F) state of Fig. 4(a).

Two states with a zero total magnetization are coplanar ($H_c^S = \mathbb{Z}_2$):

(ii) The $\mathbf{q} = \mathbf{0}$ state of Fig. 4(b) has three sublattices of spins at 120° and a three-site unit cell.

(iii) The $\sqrt{3} \times \sqrt{3}$ state of Fig. 4(c) has three sublattices of spins at 120° and a nine-site unit cell.

Three states with a zero total magnetization completely break O(3) ($H_c^S = \{I\}$):

(iv) The octahedral state of Fig. 4(d) has six sublattices of spins oriented toward the corners of an octahedra and a 12-site unit cell.

(v) The cuboc1 state of Fig. 4(e) has 12 sublattices of spins oriented toward the corners of a cuboctahedron and a 12-site unit cell.

(vi) The cuboc2 state of Fig. 4(f) has 12 sublattices of spins oriented toward the corners of a cuboctahedron and a 12-site unit cell. Note that the first-neighbor spins have relative angles of 60°, in contrast to 120° for the cuboc1 state.

Two continua of states with a nonzero total magnetization completely break O(3) ($H_c^S = \{I\}$):

(vii) The $\mathbf{q} = \mathbf{0}$ umbrella states of Fig. 4(g), left.

(viii) The $\sqrt{3} \times \sqrt{3}$ umbrella states of Fig. 4(g), right.

These continua interpolate between the ferromagnetic state and the coplanar states, Figs. 4(b) and 4(c).

B. Honeycomb lattice

All the RMO's on the honeycomb lattice are depicted in Fig. 5 and listed below. The EBZ is drawn with thin lines (its surface is three times larger than that of the BZ).

Two RMO's are collinear [$H_c^S = \mathrm{O}(2)$]:

(i) The ferromagnetic state of Fig. 5(a).

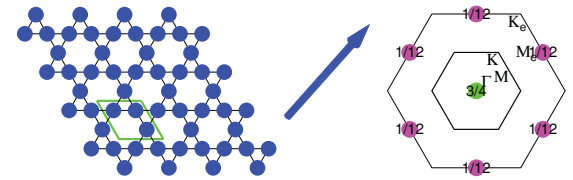

(a) Ferromagnetic (F) state.
$E = 4J_1 + 4J_2 + 2J_3' + 4J_3$.

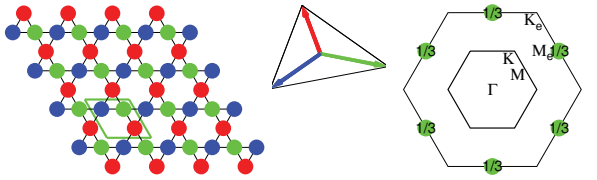

(b) $\mathbf{q} = \mathbf{0}$ state. $E = -2J_1 - 2J_2 + 2J_3' + 4J_3$.

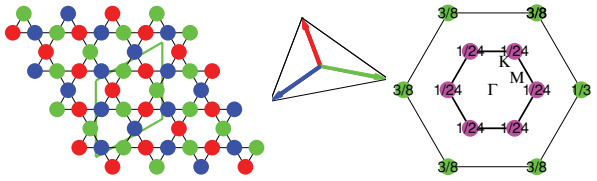

(c) $\sqrt{3} \times \sqrt{3}$ state. $E = -2J_1 + 4J_2 - J_3' - 2J_3$.

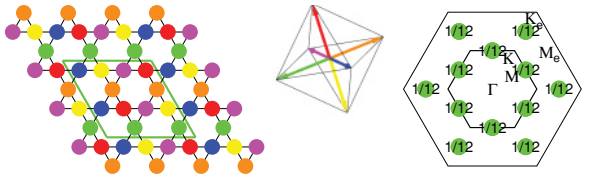

(d) Octahedral state. $E = 2J_3' - 4J_3$.

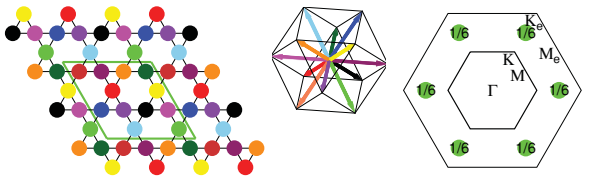

(e) Cuboc1 state. $E = -2J_1 + 2J_2 - 2J_3'$.

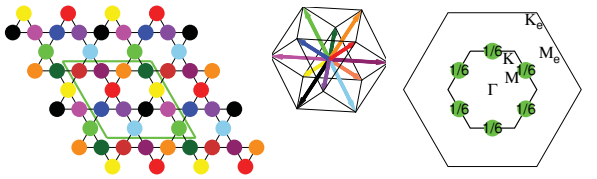

(f) Cuboc2 state. $E = 2J_1 - 2J_2 - 2J_3'$.

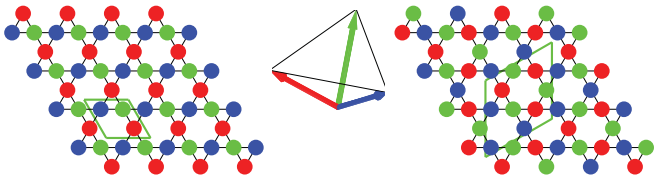

(g) $\mathbf{q} = \mathbf{0}$ (left) and $\sqrt{3} \times \sqrt{3}$ (right) umbrella states.

FIG. 4. (Color online) Regular magnetic orders on the kagome lattice and their equal-time structure factors in the EBZ (see text). The energies (per site) of these states are given for the J_1-J_2-J_3-J_3' model described in Sec VI.

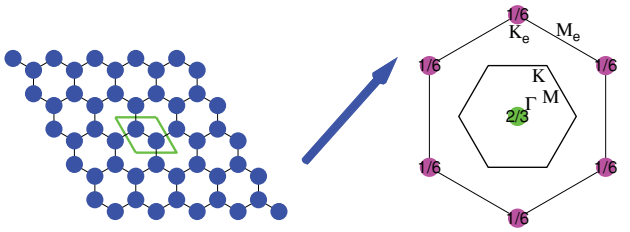

(a) Ferromagnetic (F) state. $E = 3J_1 + 6J_2 + 3J_3$.

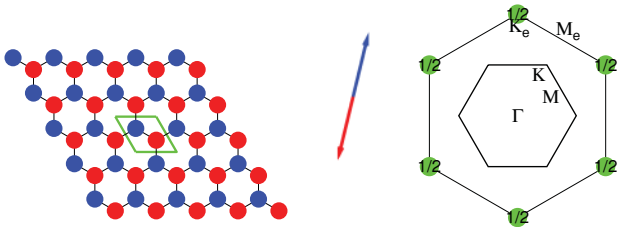

(b) Antiferromagnetic (AF) state. $E = -3J_1 + 6J_2 - 3J_3$.

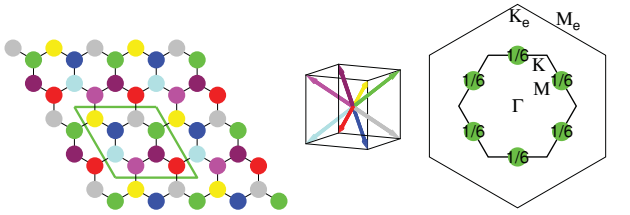

(c) Cubic state. $E = J_1 - 2J_2 - 3J_3$.

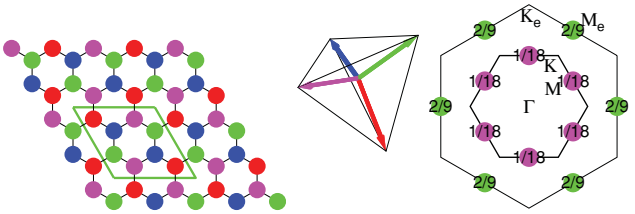

(d) Tetrahedral state. $E = -J_1 - 2J_2 + 3J_3$.

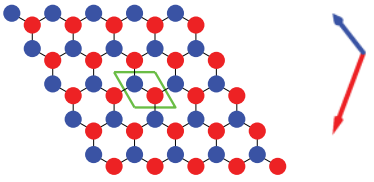

(e) V states.

FIG. 5. (Color online) Regular magnetic orders on the honeycomb lattice and their equal-time structure factors in the EBZ (see text). The energies (per site) are given for a J_1-J_2-J_3 Heisenberg model.

(ii) The antiferromagnetic state of Fig. 5(b) has two sublattices of spins oriented in opposite directions and a two-site unit cell.

Two states with a zero total magnetization completely break O(3) ($H_c^S = \{I\}$):

(iii) The cubic state of Fig. 5(c) has eight sublattices of spins oriented toward the corners of a cube and an eight-site unit cell.

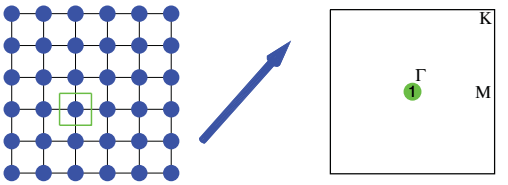

(a) Ferromagnetic (F) state.
$E = 4J_1 + 4J_2 + 4J_3 + 14K$.

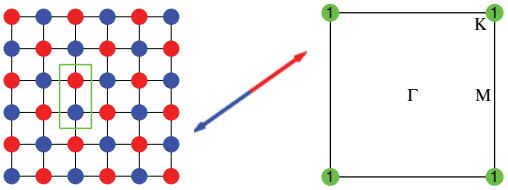

(b) (π, π) Néel (AF) state.
$E = -4J_1 + 4J_2 + 4J_3 - 2K$.

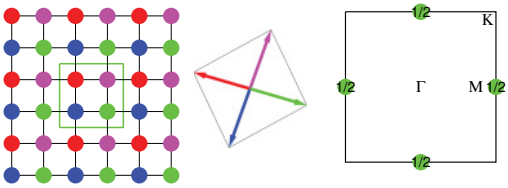

(c) Orthogonal coplanar state.
$E = -4J_2 + 4J_3 - 6K$.

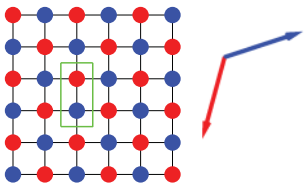

(d) V states.

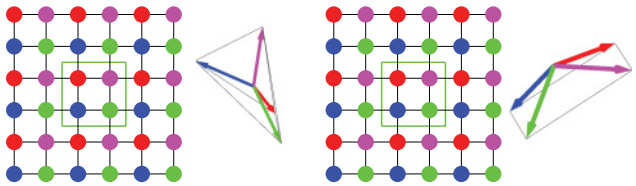

(e) Tetrahedral umbrella states (AF *umbrellas*).

(f) Umbrella states (F *umbrellas*).

FIG. 6. (Color online) Regular magnetic orders on the square lattice and their equal-time structure factors in the square BZ. The energy per site of each structure is given as a function of the parameters of the models described in Sec. VI.

(iv) The tetrahedral state of Fig. 5(d) has four sublattices of spins oriented toward the corners of a tetrahedron and a four-site unit cell.

A continuum of states with a nonzero total magnetization partially breaks O(3) ($H_c^S = \mathbb{Z}_2$):

(v) The V states of Fig. 5(e), which interpolate between the F and AF states.

C. Square lattice

The symmetry group S_L of the square lattice is distinct from that of the triangular lattice (see Fig. 2) and one has to determine its algebraic symmetry groups from a system of equations similar to Eqs. (7). The 168 solutions are listed below:

$$
\begin{aligned}
G_{T_1} = G_{T_2} = \varepsilon_1 I, \quad & G_\sigma = \varepsilon_\sigma R_{z\pi}, \quad & G_{R_4} = \varepsilon_R R_{x\pi}, \\
G_{T_1} = G_{T_2} = \varepsilon_1 R_{\mathbf{z}\pi\delta_1}, \quad & G_\sigma = \varepsilon_\sigma R_{\mathbf{x}\pi}, \quad & G_{R_4} = \varepsilon_R R_{\mathbf{z}\frac{\pi}{2}}, \\
G_{T_1} = G_{T_2} = \varepsilon_1 R_{\mathbf{z}\pi\delta_1}, \quad & G_\sigma = \varepsilon_\sigma R_{\mathbf{z}\pi\delta_\sigma}, \quad & G_{R_4} = \varepsilon_R R_{\mathbf{z}\pi\delta_R}, \\
G_{T_1} = G_{T_2} = \varepsilon_1 R_{\mathbf{z}\pi}, \quad & G_\sigma = \varepsilon_\sigma R_{\mathbf{z}\pi\delta_\sigma}, \quad & G_{R_4} = \varepsilon_R R_{\mathbf{x}\pi}, \\
G_{T_1} = G_{T_2} = \varepsilon_1 R_{\mathbf{z}\pi}, \quad & G_\sigma = \varepsilon_\sigma R_{\mathbf{x}\pi}, \quad & G_{R_4} = \varepsilon_R R_{\mathbf{z}\pi\delta_R}, \\
G_{T_1} = G_{T_2} = \varepsilon_1 R_{\mathbf{z}\pi}, \quad & G_\sigma = \varepsilon_\sigma R_{\mathbf{x}\pi}, \quad & G_{R_4} = \varepsilon_R R_{\mathbf{x}\pi}, \\
G_{T_1} = G_{T_2} = \varepsilon_1 R_{\mathbf{z}\pi}, \quad & G_\sigma = \varepsilon_\sigma R_{\mathbf{x}\pi}, \quad & G_{R_4} = \varepsilon_R R_{\mathbf{y}\pi}, \\
G_{T_1} = \varepsilon_1 R_{\mathbf{x}\pi}, \quad & G_{T_2} = \varepsilon_1 R_{\mathbf{y}\pi}, &
\end{aligned}
$$

$$
G_\sigma = \begin{pmatrix} 0 & 1 & 0 \\ 1 & 0 & 0 \\ 0 & 0 & -\varepsilon_\sigma \end{pmatrix}, \quad G_{R_4} = \begin{pmatrix} 0 & e_1 & 0 \\ e_2 & 0 & 0 \\ 0 & 0 & e_3 \end{pmatrix},
$$

where $\mathbf{x}$, $\mathbf{y}$, $\mathbf{z}$ are orthonormal vectors, e_1, e_2, e_3, ε_1, ε_σ, $\varepsilon_R = \pm 1$, and δ_R, δ_σ, $\delta_1 = 0$ or 1.

Then, the construction of the compatible states leads to the RMO's depicted in Fig. 6 and listed below.

Two RMO's are collinear [$H_c^S = \mathrm{O}(2)$]:

(i) The ferromagnetic state of Fig. 6(a).

(ii) The (π,π) Néel (AF) state of Fig. 6(b) has two sublattices of spins oriented in opposite directions and a two-site unit cell.

One state with a zero total magnetization is coplanar ($H_c^S = \mathbb{Z}_2$):

(iii) The orthogonal coplanar state of Fig. 6(c) has four sublattices of spins with angles of 90° and a four-site unit cell.

Then we have three continua of states:

(iv) The V states of Fig. 6(d) have a nonzero total magnetization and partially break O(3) ($H_c^S = \mathbb{Z}_2$). They interpolate between the F and the (π,π) Néel states.

(v) The tetrahedral umbrella states of Fig. 6(e) have a zero total magnetization and completely break O(3) ($H_c^S = \{I\}$). They interpolate between the (π,π) Néel and the orthogonal coplanar state.

(vi) The four-sublattice umbrella states of Fig. 6(f) have a nonzero total magnetization and completely break O(3) ($H_c^S = \{I\}$). They interpolate between the F and the orthogonal coplanar state.

D. Regular magnetic orders with only translations

When the lattice symmetry group is commutative, the construction of RMO's is particularly simple. This occurs if only translations are considered. In that case, one may choose some arbitrary directions for the spins of the reference unit cell. Then, one has to choose an O(3) element G_{T_i} associated with each unit lattice translation T_i in direction i (with as many generators as space dimensions). Assuming that $H_c^S = I$, and using the fact that the translations commute with each other,

we find that the G_{T_i} also commute. A first family of solutions consists in choosing a set of rotations with the same axis $\mathbf{n}$, and unconstrained angles. This gives the conventional spiral states. Thanks to the arbitrary choice of the spin directions in the reference unit cell, such states are not necessarily planar.

All these solutions may be generalized by combining one or more G_{T_i} with a spin inversion $-I$. These generalized spiral states will be denoted SS's in the following.

Finally, another family of solutions can be obtained by choosing the G_{T_i} among the set of π rotations with respect to some orthogonal spin directions, therefore insuring the commutativity regardless of whether or not they are combined with $-I$.

V. GEOMETRICAL REMARKS

In this section, we discuss some geometrical properties of RMO's.

A. Groups and polyhedra

From an RMO c, one can consider the set $\Sigma \subset \mathcal{A}$ of all the different orientations taken by the spins. We assume that c has a finite number of sublattices (and thus of spin directions), so that Σ is finite. For a three-component spin system, Σ is just a set of points on the unit sphere $\mathcal{S}_2$, as displayed in the central columns of Figs. 3, 4, 5, and 6. Σ may be a single site, the ends of a segment, the corners of a polygon, or the corners of a polyhedra.

The four lattices studied here share some special properties: all the sites and all first-neighbor bonds are equivalent (linked by an S_L transformation). Due to this equivalence, Σ also forms a segment-polygon-polyhedron with equivalent vertices and bonds (notice that nearest neighbors on the lattice do not necessarily correspond to nearest neighbor spin directions in spin space). A polyhedron with this property is said to be quasiregular. If the elementary plaquettes of the lattices are also equivalent (as in the triangular, square, and hexagonal lattices, but not in the kagome lattice where both triangular and hexagonal elementary plaquettes are present) and if Σ is a polyhedron, its faces should also be equivalent. Σ must then be one of the five regular convex polyhedra (Platonic solids):[6] tetrahedron, cube, octahedron, dodecahedron, or icosahedron (again, the plaquettes of the lattice need not to map to the faces of the polyhedron).

We now only consider the case in which $H_c^S = \{I\}$ (this condition can always be verified by reducing $\mathcal{A}$ to its elements invariant by H_c^S and by consequently modifying S_S). Clearly, the lattice symmetries constrain the possibilities for the set Σ, since each lattice symmetry X permutes the sites in Σ but leaves it globally unchanged. This relation is particularly easy to visualize in the case of the tetrahedral state on the triangular lattice, since both the lattice and the polyhedron Σ have triangular plaquettes (faces): one can put a tetrahedron with a face posed onto a lattice face. Then, one *rolls* the tetrahedron over the lattice to obtain a spin direction at each lattice site. Notice that such a construction would *not* work with a cube on the square lattice (and indeed, there is no such eight-sublattice RMO on the square lattice; see Sec. IV C). But since the state c is regular, these permutations can also be achieved by a spin symmetry in S_S, and the symmetry group S_Σ of Σ should be viewed as a finite subgroup of S_S.

For $S_S = \mathrm{O}(3)$, the classification of these subgroups—called point groups—is a classical result in geometry.[6] It contains seven groups (related to the three symmetry groups of the five regular polyhedra) and seven infinite series (conventionally denoted C_n, C_{nv}, C_{nh}, D_n, D_{nh}, D_{nd}, and S_n with $n \in \mathbb{N}$; they are related to the cyclic and dihedral groups). Of course, the nonplanar RMO's we have discussed so far (Secs. III C and IV) fall into this classification. For instance, the three- and four-sublattice umbrella states of Figs. 3(d), 6(e), and 6(f) correspond to C_{3v}, D_{2d}, and C_{4v} (with six, eight, and eight elements, respectively). The cubic, octahedral, and cuboctahedron states correspond to the symmetry group of the cube (48 elements), and the tetrahedral state corresponds (of course) to its own symmetry group.

B. Regular magnetic orders and representation of the lattice symmetry group

We again focus on three-component spin systems with a spin symmetry group $S_S = \mathrm{O}(3)$. In an RMO c, each lattice symmetry X can be associated to a matrix G_X in O(3). Now, as in Sec. III A, we can compare the actions of two lattice symmetries X and Y. $G_X G_Y G_{XY}^{-1}$ belongs to H_c^S. By choosing G_X invariant in all directions perpendicular to all spins, we obtain $G_X G_Y = G_{XY}$, which implies that G is a *representation* of the lattice symmetry group S_L. After removing the trivial representations associated with directions perpendicular to spins, its dimension is 1 for a collinear state, 2 for planar states, and 3 for the others. Is this representation reducible? If yes, it must contain at least one representation of dimension 1 (because the maximal dimension considered here is 3), thus there exists at least one spin direction that is stable under all the spin symmetry operations spanned by G_X with $X \in S_L$. Except in the trivial collinear case, one can easily check that it is the case only for the states belonging to a continuum. For the V states, G is the direct sum of a trivial and a nontrivial 1D representation of S_L. For the umbrella states, G is the direct sum of a trivial 1D and a 2D irreducible representation (IR). For the tetrahedral state of Fig. 6(e), G is the direct sum of a nontrivial 1D and a 2D IR representation. For the other cases, the associated representation is irreducible.

There is another context in which antiferromagnetic Néel states are known to be related to irreducible representations. If a quantum antiferromagnet has a GS with long-range Néel order, its spectrum displays a special structure, called a "tower of states."[7,8] It reflects the fact that a symmetry-breaking Néel state is a linear combination of specific eigenstates with different quantum numbers describing the spatial symmetry breaking, and with different values of the total spin S, describing the SU(2) symmetry breaking. If such a quantum system has a GS with a regular Néel order, its tower of state should have an $S = 1$ state with the same quantum numbers as those of the irreducible representation $X \mapsto G_X$ discussed above. The reason why this representation shows up in the $S = 1$ sector of the tower of state is because $S = 1$ corresponds to the action of the lattice symmetries onto a three-dimensional vector, as in the classical spin directions.

VI. ENERGETICS

As discussed in the Introduction, there is no simple way to find the GS of a classical spin model if the lattice is not a Bravais lattice, and/or if spin-spin interactions are not simply quadratic in the spin components. So far, we have discussed RMO's from pure symmetry considerations, but in Sec. VI A we show that, under some rather general conditions, a RMO is a *stationary* point for the energy, regardless of the Hamiltonian (provided it commutes with the lattice symmetries).

In addition, we argue that RMO's are good candidates to be *global energy minima*. To justify this, we first discuss a rigorous energy lower bound (Sec. VI B) for Heisenberg-like Hamiltonians, and we investigate in Sec. VI C several Heisenberg models with further neighbor interactions (J_1, J_2, J_3, etc.) on non-Bravais lattices such as the hexagonal and kagome lattices. In large regions of the phase diagrams, one RMO energy reaches the lower bound and is one (possibly not unique) exact GS.

A. A condition for an RMO to be "stationary" with respect to small spin deviations

To address the question of the energetic stability of RMO's, we give some conditions under which an infinitesimal variation of the spin directions would not change the energy (a necessary condition to have a GS). To simplify the notations, we consider a Heisenberg model with some competing interactions [such as in Eq. (1)], but the arguments easily generalize to multispin interactions of the form $(\mathbf{S}_i \cdot \mathbf{S}_j)(\mathbf{S}_k \cdot \mathbf{S}_l) \ldots$ (at the condition that they respect the lattice symmetries).

We assume that there is a nontrivial lattice symmetry X that leaves one site i unchanged: $X(i) = i$ (existence of a nontrivial point group). In addition, we assume that a spin rotation R_s of axis $\mathbf{n}$ and angle $\theta \neq 0$ can be associated with X to have $R_s X c = c$. These conditions ensure that the invariant direction of R_s is $\mathbf{n} = \pm\mathbf{S}_i$. With the exception of states belonging to a continuum, all RMO's verify these conditions on the lattices we have studied.

With these conditions, the derivatives of the energy with respect to the spin directions vanish. The proof is as follows. One considers the local field $\mathbf{h}_i = \frac{\partial E}{\partial \mathbf{S}_i}$, which is experienced by the spin i. $\mathbf{h}_i$ is a linear combination of the $\mathbf{S}_j$ where j runs over the sites that interact with the site i:

$$\mathbf{h}_i = \sum_d J_d \sum_{j \in N_d(i)} \mathbf{S}_j, \tag{12}$$

where $N_d(i)$ is the set of the neighbors of i at distance d on the lattice. Since the configuration c is invariant under $R_s X$, one may also compute $\mathbf{h}_i$ as

$$\mathbf{h}_i = \sum_d J_d \sum_{j \in X(N_d(i))} R_s(\mathbf{S}_j). \tag{13}$$

X reshuffles the neighbors of i (at any fixed distance), but since $X(i) = i$, $N_d(i)$ is globally stable: $N_d(i) = X(N_d(i))$. So, from Eq. (13), we have

$$\mathbf{h}_i = R_s(\mathbf{h}_i). \tag{14}$$

We therefore conclude that $\mathbf{h}_i$ is collinear with $\mathbf{n}$ and thus collinear with $\mathbf{S}_i$. This shows that the energy derivative $\frac{\partial E}{\partial \mathbf{S}_i}$ vanishes for spin variations orthogonal to $\mathbf{S}_i$ [longitudinal spin variations are not allowed as $(\mathbf{S}_i)^2$ must be kept fixed].

All RMO's studied in the previous examples that do not belong to a continuum are thus "energetically stationary" with respect to small spin deviations. They are thus interesting candidates for global energy minima.

B. Lower bound on the energy of Heisenberg models

The Fourier transform $\mathbf{S}_{\mathbf{q}i}$ of the local spin on a periodic lattice of N unit cells is defined by

$$\mathbf{S}_{\mathbf{q}i} = \frac{1}{\sqrt{N}} \sum_{\mathbf{x}} \mathbf{S}_{\mathbf{x}i} e^{-i\mathbf{q}\mathbf{x}},$$

where each site is labeled by an index $i = 1, \ldots, m$ (m is the number of sites per unit cell), $\mathbf{x}$ is the position of its unit cell, and $\mathbf{q}$ is a wave vector in the first Brillouin zone. For a Hamiltonian in the form of Eq. (1), the energy can be written as

$$E = \sum_{\substack{\mathbf{v},\mathbf{x} \\ i,j=1,\ldots,m}} J_{ij}(\mathbf{v})\, \mathbf{S}_{\mathbf{x}i} \cdot \mathbf{S}_{\mathbf{x}+\mathbf{v}j} \tag{15}$$

$$= \sum_{\substack{\mathbf{q} \in \mathrm{BZ} \\ i,j=1,\ldots,m}} J_{ij}(\mathbf{q})\, \mathbf{S}_{-\mathbf{q}i} \cdot \mathbf{S}_{\mathbf{q}j}, \tag{16}$$

with

$$J_{ij}(\mathbf{q}) = \sum_{\mathbf{v}} J_{ij}(\mathbf{v}) e^{i\mathbf{q}\cdot\mathbf{v}}. \tag{17}$$

Since $(\mathbf{S}_{i\mathbf{x}})^2 = 1$ for all i and $\mathbf{x}$, $\sum_{i\mathbf{x}} \mathbf{S}_{i\mathbf{x}}^2 = \sum_{i\mathbf{q}} \mathbf{S}_{q\mathbf{x}}^2 = mN$, we see that a lower bound on the energy (per site) is obtained from the lowest eigenvalue of the matrices $J(\mathbf{q})$:[9]

$$\frac{E}{mN} \geqslant \min_{\{\mathbf{q}\}} \left(J_{\mathbf{q}}^{\min}\right), \tag{18}$$

where $J_{\mathbf{q}}^{\min}$ is the lowest eigenvalue of the matrix $J(\mathbf{q})$.

If the lattice has a single site per unit cell ($m = 1$), this lower bound is reached by a planar spiral of the form[1]

$$\mathbf{S}_{\mathbf{x}1} = \mathbf{u}\cos(\mathbf{Q}\cdot\mathbf{x}) + \mathbf{v}\cos(\mathbf{Q}\cdot\mathbf{x}), \tag{19}$$

where $\mathbf{Q}$ is the propagation vector (pitch) of the spiral, and corresponds to a minimum of $J_{\mathbf{q}}^{\min}$. In spin space, the plane of the spiral is fixed by two orthonormal vectors $\mathbf{u}$ and $\mathbf{v}$. When $m = 1$, it is only when $J_{\mathbf{q}}^{\min}$ admits several degenerate minima in the Brillouin zone that additional nonspiral (and possibly nonplanar) GS's may be constructed. If the lattice has more than one site per unit cell, an attempt to construct a spiral with a pitch corresponding to the smallest eigenvalue $J(\mathbf{Q})^{\min}$ will generally *not* lead to a physical spin configuration with fixed spin length $\mathbf{S}_{i\mathbf{x}}^2 = 1$ at every site. We will, however, see in the next section that for some models, a nonplanar RMO may reach the lower bound, whereas all the spiral states are energetically higher.

C. Variational phase diagrams of Heisenberg models on the kagome and hexagonal lattices

In this section, we comment on the phase diagrams of J_1-J_2-J_3($-J_3'$) Heisenberg models on the kagome and hexagonal lattices. J_n is the interaction between nth neighbors. On the

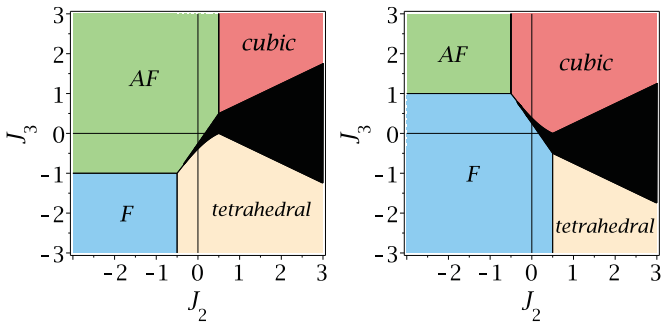

FIG. 7. (Color online) Phase diagram of the J_1-J_2-J_3 Heisenberg model on the honeycomb lattice. Labels refer to the RMO's described in Fig. 5. In each colored region (black excluded), the RMO is an exact GS. In the black region, a generalized spiral state (SS) has an energy strictly lower than the RMO's, but the actual GS energy might still be lower.

kagome lattice, there are two types of third neighbors depicted in Fig. 8(a), and thus two coupling constants J_3 and J_3'.

For each set of parameters, we determined the lowest-energy RMO (the energies of RMO's are given in Figs. 4 and 5), the lowest-energy SS of Sec. IV D, and the lower bound on the energy. The results on these two lattices are described in Figs. 7 and 8. Such phase diagrams are *a priori* variational. However, it turns out than in all the colored (white included, gray and black excluded) regions of Figs. 7 and 8, the RMO with the lowest energy reaches the rigorous lower energy bound of Eq. (18). *This demonstrates that (at least) one GS is regular in these regions of the parameter space.* In the gray areas, the energy lower bound is not reached, but the regular nearby state could be a GS as no SS has a lower energy. In the black areas, the GS is not regular: some SS's are energetically lower (but sometimes still higher than the lower bound). All RMO's (excepted those from continua) appear in some area of the presented phase diagrams. This shows that these states are good candidates as variational GS's. The absence of RMO's of a continuum in a Heisenberg model is easily understood. The energy E of any RMO c belonging to a continuum cannot be lower than the energies E_1 and E_2 of the two states c_1 and c_2 between which it interpolates. One (at least) of the two states, say c_1, is collinear along a direction $\mathbf{n}$. The c_2 spins are then perpendicular to $\mathbf{n}$. Let θ be the angle between the spins of the continuum state and $\mathbf{n}$. Then $\mathbf{S}_i = \mathbf{S}_i^{c_1}\cos\theta + \mathbf{S}_i^{c_2}\sin\theta$ and the energy reads $E = E_2 + (E_1 - E_2)\cos^2\theta$. Thus, E is in between E_1 and E_2 and is never strictly the lowest energy. In the presence of an external magnetic field $\mathbf{h}$ and if a one-dimensional representation included in G is ferromagnetic (as is the case for some umbrellas and for the V states), $\mathbf{n}$ aligns on $\mathbf{h}$. The energy then reads $E = E_2 + (E_1 - E_2)\cos^2\theta - \mathbf{h}\cos\theta$ and an umbrella state becomes stationary. It is well known that such a structure can be the GS in the presence of a magnetic field.[10,11]

We will now address the possible degeneracies of regular tridimensional spin states in these models. On the hexagonal lattice, our phase diagram is in agreement with Ref. 12. One should nevertheless notice that the regular tridimensional orders (tetrahedral and cubic states) are degenerate with collinear

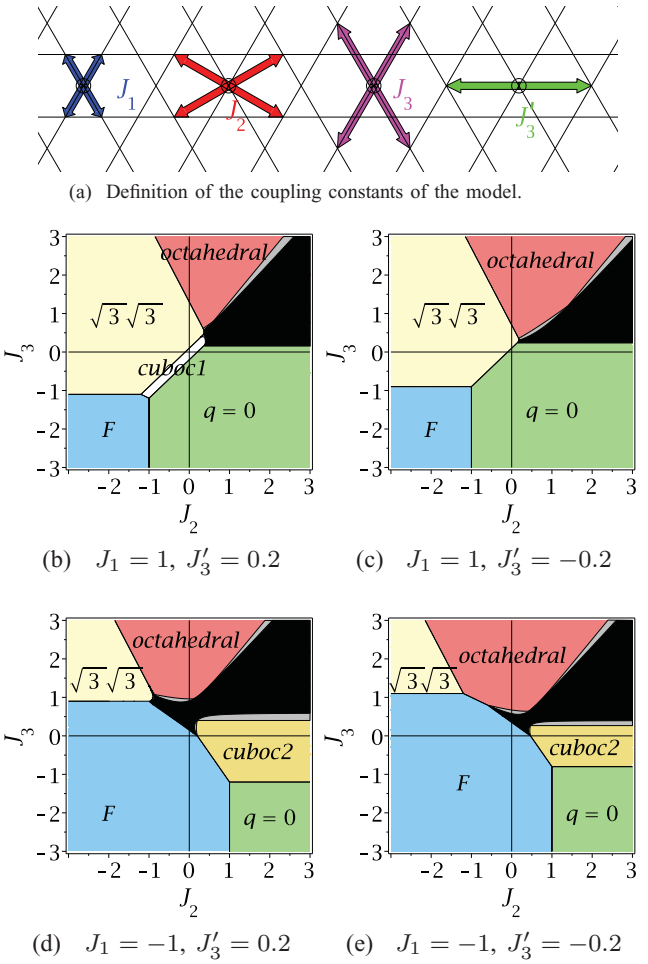

FIG. 8. (Color online) Phase diagram of the J_1-J_2-J_3-J_3' model on the kagome lattice. In each colored region (white included, gray and black excluded), the RMO is an exact GS. Labels refer to the RMO's described in Fig. 4. In the gray regions, the nearby RMO does not reach the lower bound of Sec. VI B, but no SS is energetically lower. In the black regions, an SS has a lower energy than the RMO's, but the actual GS might yet be lower.

non-RMO's. These last states have a higher density of soft excitations (larger energy wells in the phase-space landscape) and will always win as soon as (thermal or quantum) fluctuations are introduced (order by disorder mechanism[13–17]). However, the nonplanar configurations could be stabilized by quartic or ring-exchange interactions.

On the kagome lattice (Fig. 8), the occurrence of the cuboc2 [Fig. 4(f)] for J_1-J_2 interactions[18] and of the cuboc1 [Fig. 4(e)] for J_1-J_3' interactions[19] has already been reported. These two states are not degenerated with SS's and are to the best of our knowledge unique and stable GS's of the model. The octahedral state has not been found before, but this state has the same energy as a continuum of non-SS's including collinear states, and it will be destabilized by any fluctuation.

D. Square and triangular lattices: Phase diagrams of Heisenberg versus ring-exchange models

In this section, we will comment on the phase diagram of the Heisenberg models [Eq. (1)] on the square and triangular

lattices and display the effect of four-spin ring-exchange (J_1-J_2-K) on these two lattices. The J_1-J_2-K model is defined as

$$E = \sum_{i,j} J(|\mathbf{x}_i - \mathbf{x}_j|)\mathbf{S}_i \cdot \mathbf{S}_j + K \sum_{i,j,k,l} [(\mathbf{S}_i \cdot \mathbf{S}_j)(\mathbf{S}_k \cdot \mathbf{S}_l) + (\mathbf{S}_i \cdot \mathbf{S}_l)(\mathbf{S}_j \cdot \mathbf{S}_k) - (\mathbf{S}_i \cdot \mathbf{S}_k)(\mathbf{S}_j \cdot \mathbf{S}_l) + \mathbf{S}_i \cdot \mathbf{S}_j + \mathbf{S}_j \cdot \mathbf{S}_k + \mathbf{S}_k \cdot \mathbf{S}_l + \mathbf{S}_l \cdot \mathbf{S}_i + \mathbf{S}_i \cdot \mathbf{S}_k + \mathbf{S}_j \cdot \mathbf{S}_l], \quad (20)$$

where the sum in the K term runs on rhombi i,j,k,l.[2] This model encompasses first- and second-neighbor J_1 and J_2 couplings and a K is ring-exchange term that introduces quartic interactions as well as modifications of first- and second-neighbor Heisenberg interactions.[2] The phase diagrams are displayed in Figs. 9 and 10.

In the J_1-J_2-J_3 Heisenberg phase diagrams on the square and triangular lattice, all RMO's that do not belong to continua do appear as an exact GS in some parts of the phase diagrams [colored regions except for the black areas in Figs. 9(a), 9(b), 10(a), and 10(b)]. In the black regions, SS's are more stable than RMO's. As these lattices are Bravais lattices, we know how to reach the lower bond of Sec. VI B thanks to a spiral state. The orthogonal state on the square lattice and the tetrahedral state on the triangular lattice [Figs. 3(b) and 6(c)] are degenerate with SS's including collinear states with two spins (up, down) in the magnetic unit cell, which will win upon introduction of fluctuations. On a large part of the phase diagram on the square lattice (spirals excepted), the spins are thus collinear.

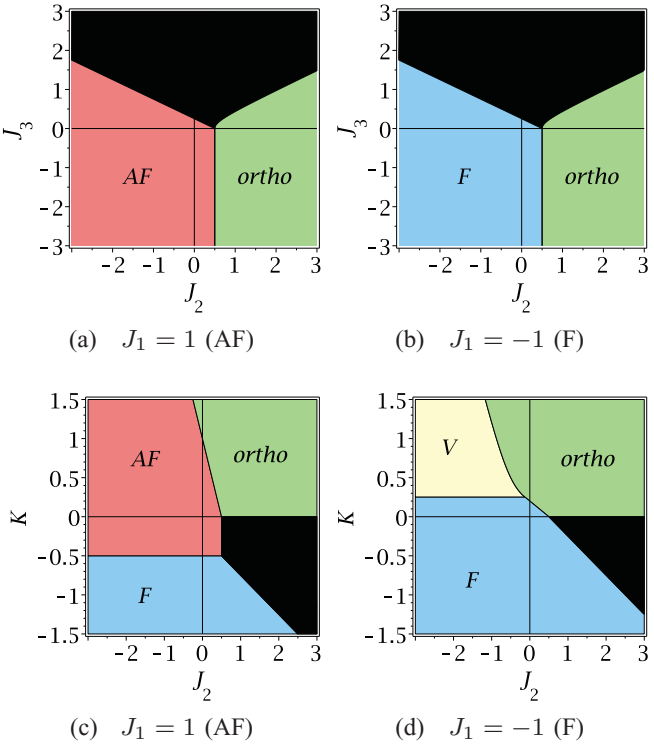

(a) $J_1 = 1$ (AF) (b) $J_1 = -1$ (F)

(c) $J_1 = 1$ (AF) (d) $J_1 = -1$ (F)

FIG. 9. (Color online) Phase diagrams on the square lattice with J_1-J_2-J_3 Heisenberg interactions (top line) and J_1-J_2-K model (bottom line). Labels refer to RMO's defined in Fig. 6. In each colored region (black excepted), the RMO has the lowest energy of the set of all regular and generalized spiral states. In the black regions, an SS has a lower energy than the RMO's. For pure Heisenberg interactions, we know that we obtain the GS energy, but for non-Heisenberg interactions the actual GS might be lower. In the J_1-J_2-J_3 model, the coplanar (orthogonal four-sublattice) phase is degenerate with nonregular collinear states, which will win upon introductions of fluctuations. On the contrary, the coplanar (orthogonal four-sublattice) phase is stable in a large range of parameters in the J_1-J_2-K model.

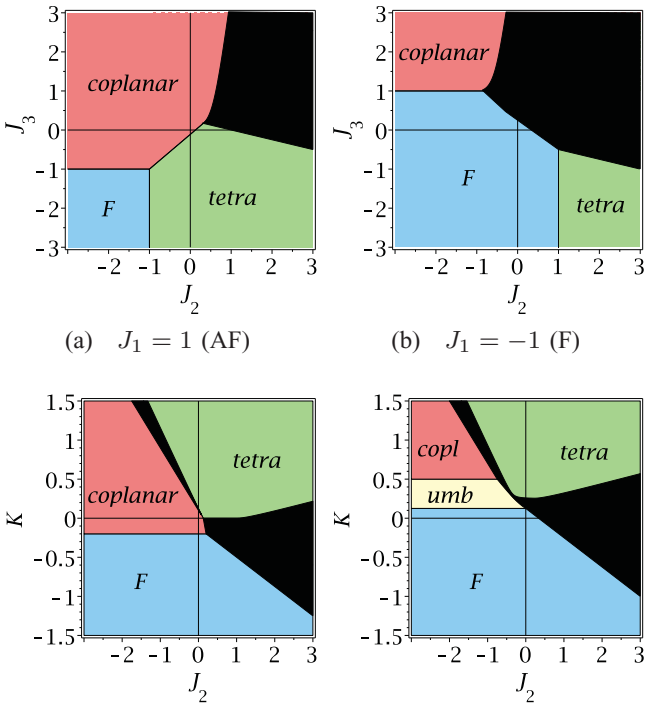

(a) $J_1 = 1$ (AF) (b) $J_1 = -1$ (F)

(c) $J_1 = 1$ (AF) (d) $J_1 = -1$ (F)

FIG. 10. (Color online) Phase diagrams on the triangular lattice with J_1-J_2-J_3 Heisenberg interactions (top line) and J_1-J_2-K model (bottom line). Labels refer to RMO's defined in Fig. 3. In each colored region (except black), the RMO has the lowest energy of the set of all regular and generalized spiral states. In the black regions, an SS has a lower energy than the RMO's. For pure Heisenberg interactions, we know that we obtain the GS energy, but for non-Heisenberg interactions the actual GS might be lower.

The presence of a four-spin ring exchange on the square lattice gives richer phase diagrams [Figs. 9(c) and 9(d)] with the appearance of states from continua. We recall that these phase diagrams are variational and give the minimal energy state among the regular and generalized spiral states. A dominant four-spin ring exchange stabilizes the orthogonal four-sublattice coplanar antiferromagnet, which is known to be robust to large quantum fluctuations.[20] One of these phases belongs to a continuum: the V states [Fig. 6(d)]. Part of this phase diagram on the square lattice has been known for a long time for the J_1-K model,[21] but the effect of a second-neighbor interaction leads to new phases that might be interesting in various respects.

The J_1-J_2-K phase diagram on the triangular lattice [Figs. 10(c) and 10(d)] exhibits all the regular phases that can be constructed on this lattice. In that model, large ring

exchange stabilizes the tetrahedral chiral phase studied by Momoi and co-workers.[2,22] The presence of large parts of the phase diagrams with a planar or three-dimensional order parameter at $T = 0$, and of points where a large number of classical phases are in competition, could give interesting hints in the quest of exotic quantum phases.[23–25]

E. Finite-temperature phase transitions in two dimensions

In two dimensions, the Mermin-Wagner[26] theorem insures that continuous symmetries cannot be spontaneously broken at finite temperature. It does not, however, prevent discrete symmetries from being broken. Indeed, some finite-temperature phase transitions associated with discrete symmetries have been found in classical O(3) models: lattice symmetry breaking in the J_1-J_2 and J_1-J_3 models on the square lattice,[27–29] and chiral symmetry breaking in a ring-exchange model on the triangular lattice[17,22] and in a J_1-J_2 model on the kagome lattice.[18,30]

What should be expected in a system where the GS is an RMO c? Let us first consider the case in which c is not chiral, that is, when the spin inversion $\mathbf{S} \to -\mathbf{S}$ gives a state c' that can also be obtained from c by a rotation in SO(3). At an infinitesimal temperature, the rotational symmetry is restored and the statistical ensemble is that of all the (regular) states obtained from c by SO(3) rotations. The thermal average of an observable is therefore also an average over SO(3) rotations. Now, if we compare an observable O and the same observable after a lattice symmetry X, we will get the same average (for RMO's, the effect of X can be absorbed by a rotation). So not only the rotational symmetries but also all the lattice symmetries are restored at $T = 0^+$. The simplest scenario is therefore a complete absence of symmetry-breaking phase transition from $T = 0^+$ up to $T = \infty$. Now, for a chiral state, the thermal fluctuations will only partially restore the O(3) symmetry of the model, and a chiral phase transition should be expected. From this point of view, a classical system in two dimensions with no finite-temperature phase transition is likely to have a regular and nonchiral GS.

When some magnetic long-range order develops, the magnetoelastic couplings often drive the system to a small but detectable (through x-ray diffraction, for instance) lattice distortion. This generically happens if the magnetic order induces some inequivalent bonds, since the magnetic energy gain is then expected to be linear in the displacements, whereas the elastic energy cost is quadratic. However, such inequivalent bonds do not occur in the case of RMO's (the energy is rotationally invariant, hence uniform) and we expect the crystal to keep its full symmetry in such a magnetically ordered phase. Likewise, the absence of any lattice distortion down to zero temperature can be used as an (experimental) indication that the magnetic phase is regular.

VII. CONCLUSION

Based on symmetry considerations (and on an analogy with Wen's[3] classification of quantum spin liquids using the concept of a projective symmetry group), we introduced a family of classical magnetic structures, dubbed "regular" magnetic orders. They can be constructed in a systematic way for any lattice, in any dimension, for any type of spins, using the method explained in Sec. III. We found that these states are often good variational states to study the zero-temperature phase diagram of "complex" problems (non-Bravais lattice and/or multiple spin interactions, for instance). In many cases, one of the RMO's is found to reach a lower energy bound, allowing us to show that it is a GS.

We note that, although one can always find a planar GS in Heisenberg models on a Bravais lattice, nonplanar spin structures with many sublattices are rather common in the presence of competing interactions, nonquadratic spin interactions, and non-Bravais lattices. As mentioned in the Introduction, we believe this approach may find an application in the study of real magnetic compounds where the (equal-time) spin-spin correlations are measured, but the strength and range of the magnetic exchange interactions are not known.

We have studied the case in which the spin manifold $\mathcal{A} = \mathcal{S}_2$ is that of a three-component spin (unit vector), but other manifolds could be investigated using the same approach. For instance, *regular nematic orders* would be obtained with $\mathcal{A} = \mathcal{S}_2/\mathbb{Z}_2$ and $S_S = \mathrm{SO}(3)$.

This approach was applied here to purely classical models, but can be applied similarly to quantum systems where the spin-rotational symmetry is broken (magnetic long-range order). Appendix C describes a similar approach for the case of spin *liquids*, where no symmetry at all is broken. It is interesting to understand the connections between RMO's and (mean-field) spin liquids. In particular, an important question is to identify which spin liquid may give rise to which RMO upon spinon condensation. This issue has been addressed in Ref. 31 and will be the subject of a future publication.

ACKNOWLEDGMENTS

We thank L. Pierre for enlightening discussions on spiral states and V. Pasquier for interesting input on geometrical considerations and for mentioning Ref. 6. This research was supported in part by the National Science Foundation under Grant No. PHY05-51164.

APPENDIX A: DERIVATION OF THE ALGEBRAIC SYMMETRY GROUPS ON THE TRIANGULAR LATTICE

In this appendix, we look for all the algebraic symmetry groups on the triangular lattice with symmetries of Fig. 2. They are the solutions of the system Eq. (8) recalled here:

$$G_{T_1} G_{T_2} = G_{T_2} G_{T_1}, \tag{A1a}$$
$$G_{T_1} G_{R_6} G_{T_2} = G_{R_6}, \tag{A1b}$$
$$G_{R_6} G_{T_1} G_{T_2} = G_{T_2} G_{R_6}, \tag{A1c}$$
$$G_{T_1} G_{\sigma} = G_{\sigma} G_{T_2}, \tag{A1d}$$
$$G_{R_6}^6 = I, \tag{A1e}$$
$$G_{\sigma^2} = I, \tag{A1f}$$
$$G_{R_6} G_{\sigma} G_{R_6} = G_{\sigma}. \tag{A1g}$$

Each element G_X in $O(3)$ is characterized by its determinant $\varepsilon_X = \pm 1$ and by a rotation $R_{\mathbf{n}_X \theta_X}$ of axis $\mathbf{n}_X$ and of angle $\theta_X \in [0,\pi]$ such that $G_X = \varepsilon_X R_{\mathbf{n}_X \theta_X}$. We choose an

orthonormal right-oriented basis $(\mathbf{x},\mathbf{y},\mathbf{z})$ to express the results [such that $\mathbf{x}\cdot(\mathbf{y}\wedge\mathbf{z})=1$].

Some simple conditions on solutions are easily obtained: from Eq. (A1c) we deduce that $\varepsilon_{T_1}=1$, from Eq. (A1b) that $\varepsilon_{T_2}=1$. Equation (A1d) is a similarity relation, thus $\theta_{T_1}=\theta_{T_2}$. Equations (A1e) and (A1f) give $6\theta_{R_6}=2\theta_\sigma=0$ modulo 2π. These first results are summarized below:

$$\varepsilon_{T_1}=\varepsilon_{T_2}=1, \tag{A2a}$$
$$\theta_{T_1}=\theta_{T_2}, \tag{A2b}$$
$$\theta_\sigma\in\{0,\pi\}, \tag{A2c}$$
$$\theta_R\in\left\{0,\frac{\pi}{3},\frac{2\pi}{3},\pi\right\}. \tag{A2d}$$

The values of ε_σ and ε_{R_6} have no influence on the validity of a solution. Thus we solve Eq. (A1) only for $\varepsilon_\sigma=\varepsilon_{R_6}=1$ and then obtain all solutions by extending their values $(\varepsilon_\sigma,\varepsilon_{R_6})$ to $(\pm1,\pm1)$, keeping the other parameters $(\theta_X,\mathbf{n}_X)$ fixed.

We will divide the solutions in families depending on the relations between G_{T_1} and G_{T_2}. We immediately discern the case $\theta_{T_1}=0$ $(G_{T_1}=G_{T_2}=I)$. From now $\theta_{T_1}>0$, thus the directions $\mathbf{n}_{T_1}$ and $\mathbf{n}_{T_2}$ are uniquely defined (with only a sign ambiguity when $\theta_{T_1}=\pi$). Equation (A2a) implies that G_{T_1} and G_{T_2} are rotations and possess at least one eigenvalue equal to 1 along the directions $\mathbf{n}_{T_1}$ and $\mathbf{n}_{T_2}$. Equation (A1a) applied to vectors $\mathbf{n}_{T_1}$ gives that $G_{T_2}\mathbf{n}_{T_1}$ is an eigenvector of G_{T_1} with eigenvalue 1. If this vector is linearly independent of $\mathbf{n}_{T_1}$, then we know two independent invariant vectors of G_{T_1}. As the eigenvalue product ε_{T_1} is 1 with two eigenvalues equal to 1, we obtain that $G_{T_1}=I$, which contradicts the hypothesis $\theta_{T_1}>0$. We are left with two possibilities: $G_{T_2}\mathbf{n}_{T_1}=\pm\mathbf{n}_{T_1}$.

If $G_{T_2}\mathbf{n}_{T_1}=-\mathbf{n}_{T_1}$, then $\mathbf{n}_{T_1}$ and $\mathbf{n}_{T_2}$ are two perpendicular eigenvectors of G_{T_2} with eigenvalues -1 and 1. The third direction must correspond to the eigenvalue -1. We obtain that $\theta_1=\pi$.

If $G_{T_2}\mathbf{n}_{T_1}=\mathbf{n}_{T_1}$, then $\mathbf{n}_{T_1}=\pm\mathbf{n}_{T_2}$. Combined with Eq. (A2b), this means that $G_{T_1}=G_{T_2}$ with $\theta_{T_1}\in]0,\pi[$ or $G_{T_1}=G_{T_2}^{-1}$ with $\theta_{T_1}\in]0,\pi]$. The second subcase is incompatible with Eq. (A1c).

We obtain three families of solutions that will now be explored successively:

$$G_{T_1}=G_{T_2}=I, \tag{A3a}$$
$$\theta_{T_1}=\theta_{T_2}=\pi \text{ and } \mathbf{n}_{T_1}\perp\mathbf{n}_{T_2}, \tag{A3b}$$
$$G_{T_1}=G_{T_2}\neq I. \tag{A3c}$$

(i) In the case of Eq. (A3a), the remaining constraints are Eqs. (A1g), (A2c), and (A2d). We treat separately the two cases of Eq. (A2c).

If $G_\sigma=I$, then the possibilities for θ_R are restricted to $\{0,\pi\}$. We set $\mathbf{n}_{R_6}=\mathbf{z}$ and obtain the following two solutions:

$$G_{T_1}=G_{T_2}=I,\quad G_\sigma=I,\quad G_{R_6}=I,$$
$$G_{T_1}=G_{T_2}=I,\quad G_\sigma=I,\quad G_{R_6}=R_{\mathbf{z}\pi}.$$

If $G_\sigma=R_{\mathbf{z}\pi}$, we have the easily found solution

$$G_{T_1}=G_{T_2}=I,\quad G_\sigma=R_{\mathbf{z}\pi},\quad G_{R_6}=I,$$

and solutions with $\theta_{R_6}\neq0$. Then from Eq. (A1g) we have $G_{R_6}G_\sigma\mathbf{n}_{R_6}=G_\sigma\mathbf{n}_{R_6}$, which implies $R_{\mathbf{z}\pi}\mathbf{n}_{R_6}=\pm\mathbf{n}_{R_6}$. In the "+" case, $\mathbf{n}_{R_6}=\mathbf{z}$ and Eqs. (A1g) and (A2d) imply that $\theta_R\in\{0,\pi\}$. In the "−" case, $\mathbf{n}_{R_6}\perp\mathbf{z}$. We choose $\mathbf{n}_{R_6}=\mathbf{x}$. Equation (A1g) is verified for each θ_{R_6} of Eq. (A2d). The solutions are

$$G_{T_1}=G_{T_2}=I,\quad G_\sigma=R_{\mathbf{z}\pi},\quad G_{R_6}=R_{\mathbf{z}\pi},$$
$$G_{T_1}=G_{T_2}=I,\quad G_\sigma=R_{\mathbf{z}\pi},\quad G_{R_6}=R_{\mathbf{x}\pi/3},$$
$$G_{T_1}=G_{T_2}=I,\quad G_\sigma=R_{\mathbf{z}\pi},\quad G_{R_6}=R_{\mathbf{x}2\pi/3},$$
$$G_{T_1}=G_{T_2}=I,\quad G_\sigma=R_{\mathbf{z}\pi},\quad G_{R_6}=R_{\mathbf{x}\pi}.$$

(ii) In the case of Eq. (A3b), we choose $\mathbf{n}_{T_1}=\mathbf{x}$ and $\mathbf{n}_{T_2}=\mathbf{y}$. Equation (A1b) applied to $\mathbf{y}$, Eq. (A1c) applied to $\mathbf{z}$, Eq. (A1d) applied to $\mathbf{y}$, and Eq. (A1e) applied to $\mathbf{y}$ give the following forms for the G_{R_6} and G_σ matrices:

$$G_{R_6}=\begin{pmatrix}0&e_1&0\\0&0&e_2\\e_1e_2&0&0\end{pmatrix},\quad G_\sigma=\begin{pmatrix}0&e_3&0\\e_3&0&0\\0&0&-1\end{pmatrix},$$

where e_1, e_2, and e_3 are ±1. From Eq. (A1g) we find that $e_1=-e_3$. There remain four possibilities. But we can take $e_1=e_2=1$ up to a basis change: $(\mathbf{x},\mathbf{y},\mathbf{z})\to(e_2\mathbf{x},e_1e_2\mathbf{y},e_1\mathbf{z})$. Thus

$$G_{T_1}=R_{\mathbf{x}\pi},G_{T_2}=R_{\mathbf{y}\pi},$$
$$G_\sigma=-\begin{pmatrix}0&1&0\\1&0&0\\0&0&1\end{pmatrix},\quad G_{R_6}=\begin{pmatrix}0&1&0\\0&0&1\\1&0&0\end{pmatrix}.$$

(iii) In the last case of Eq. (A3c), we choose $\mathbf{n}_1=\mathbf{z}$. Combining Eqs. (A1b) and (A1c), we obtain that $G_{T_1}^3=I$, Thus, $G_{T_1}=G_{T_2}=R_{\mathbf{z}\frac{2\pi}{3}}$ We treat separately the two cases of Eq. (A2c).

If $G_\sigma=I$, then Eqs. (A1b) and (A1g) imply $\theta_{R_6}=\pi$. Equation (A1b) applied to $\mathbf{z}$ gives $G_{R_6}\mathbf{z}=\pm\mathbf{z}$. The "+" case ($\mathbf{n}_{R_6}=\pm\mathbf{z}$) contradicts Eq. (A1b), so it remains the "−" case: we choose $\mathbf{n}_{R_6}=\mathbf{x}$, which is a solution,

$$G_{T_1}=G_{T_2}=R_{\mathbf{z}\frac{2\pi}{3}},\quad G_\sigma=I,G_{R_6}=R_{\mathbf{x}\pi}.$$

If $\theta_\sigma=\pi$, Eq. (A1d) implies that $G_\sigma\mathbf{z}=\pm\mathbf{z}$. G_σ is either $R_{\mathbf{z}\pi}$ or a rotation of π around an axe perpendicular to $\mathbf{z}$, say $\mathbf{x}$. This last case contradicts Eq. (A1d). The only possibility is thus $G_\sigma=R_{\mathbf{z}\pi}$. From Eq. (A1b) we know that $G_{R_6}\mathbf{z}=\pm\mathbf{z}$. In the "+" case ($\mathbf{n}_{R_6}=\pm\mathbf{z}$), G_{R_6}, G_{T1}, and G_{T2} commute and Eq. (A1b) is not verified. We set $\mathbf{n}_{R_6}=\mathbf{x}$. From Eq. (A2d), only $\theta_{R_6}=\pi$ verify all the equations, giving the unique solution

$$G_{T_1}=G_{T_2}=R_{\mathbf{z}\frac{2\pi}{3}},\quad G_\sigma=R_{\mathbf{z}\pi},\quad G_{R_6}=R_{\mathbf{x}\pi}.$$

By taking into account the four solutions derived from each of the previous ones by multiplying G_σ and G_{R_6} by ±1, we finally obtained the list of solutions of Eq. (10).

APPENDIX B: POWDER-AVERAGED STRUCTURE FACTORS OF REGULAR MAGNETIC ORDERS

Equal-time spin-spin correlations partially characterize a spin state and are independent of the energetic properties of the

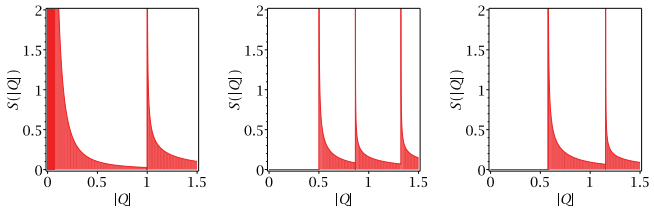

(a) F state (b) Tetrahedral state (c) Coplanar state

FIG. 11. (Color online) Powder-averaged equal-time structure factors $S(|\mathbf{Q}|)$ of the RMO's on the triangular lattice [$|\mathbf{Q}|$ is in units of 2π, $S(|\mathbf{Q}|)$ in arbitrary units].

system. Equal-time structure factors can thus be analytically calculated on RMO's to form a set of reference neutron-scattering results. They can be used to analyze measurements done on compounds with unknown GS. We define the equal-time structure factor $S(\mathbf{Q})$ of a state as

$$S(\mathbf{Q}) \propto \sum_{i,j} e^{-i\mathbf{Q}(\mathbf{x}_i-\mathbf{x}_j)}\mathbf{S}_i \cdot \mathbf{S}_j, \tag{B1}$$

where $\mathbf{x}_i$ is the position vector of the site i. The proportionality factor is adjusted to verify the sum rule $\sum_{\mathbf{Q}} S(\mathbf{Q}) = 1$. For perfect long-range orders, $S(\mathbf{Q})$ is zero everywhere except for a finite number of $\mathbf{Q}$ where Bragg peaks are present. They are broadened when chemical defects, nonzero temperature, or quantum fluctuations are taken into account.

When only powders are realizable, one can measure the powder equal-time structure factor $S(|\mathbf{Q}|)$. It is the average of $S[|\mathbf{Q}|\sin\theta(\mathbf{u}\cos\psi + \mathbf{v}\sin\psi)]$ over all the possible 3D orientations of $\mathbf{Q}$, where θ, ψ are the spherical coordinates angles of $\mathbf{Q}$ in the orthonormal basis $(\mathbf{u},\mathbf{v},\mathbf{u}\wedge\mathbf{v})$ with $\mathbf{u}$, $\mathbf{v}$ in the sample plane. Thus

$$S(|\mathbf{Q}|) \propto \int d^2\mathbf{q} \frac{\Theta(|\mathbf{Q}|-|\mathbf{q}|)}{|\mathbf{Q}|\sqrt{|\mathbf{Q}|^2-|\mathbf{q}|^2}} S(\mathbf{q}), \tag{B2}$$

where Θ is the Heaviside step function and $\mathbf{q}$ browses the reciprocal 2D space.

The equal-time structure factors $S(\mathbf{Q})$ were given in Figs. 3, 4, 5, and 6 for the RMO's on the triangular, kagome, honeycomb, and square lattices. The powder-averaged equal-time structure factors $S(|\mathbf{Q}|)$ on the triangular and kagome lattices are shown in Figs. 11 and 12.

APPENDIX C: ANALOGY WITH WEN'S PROJECTIVE SYMMETRY GROUPS (QUANTUM SPIN MODELS)

For quantum spin-$\frac{1}{2}$ Heisenberg models, a standard mean-field approximation consists in expressing the spin operators in term of fermionic operators $f_{i\alpha}$, where i is a lattice site and $\alpha = \uparrow, \downarrow$ is the spin $\pm 1/2$. A mean-field decoupling based on some bond parameters η_{ij} and ξ_{ij} (notations and details to be found in Ref. 3) can then be performed to make the Hamiltonian quadratic in the fermionic operators.

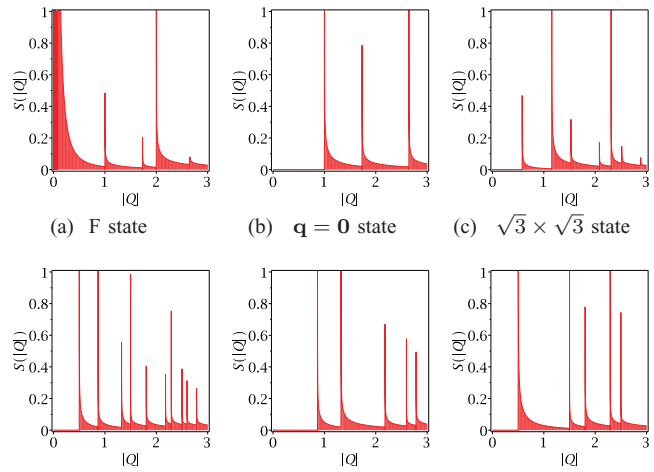

(a) F state (b) $\mathbf{q} = \mathbf{0}$ state (c) $\sqrt{3}\times\sqrt{3}$ state

(d) Octahedral state (e) Cuboc1 state (f) Cuboc2 state

FIG. 12. (Color online) Powder-averaged equal-time structure factors $S(|\mathbf{Q}|)$ of the RMO's on the kagome lattice [$|\mathbf{Q}|$ is in units of 2π, $S(|\mathbf{Q}|)$ in arbitrary units].

This theory has a local SU(2) gauge invariance. The set of gauge transformations is denoted by Φ. Physical quantities, which can be expressed using spin operators, are unaffected by a gauge transformation, although η_{ij} and ξ_{ij} are generally modified. A mean-field state is characterized by a set of η_{ij} and ξ_{ij} values, called an *Ansatz*. Two mean-field states do have the same physical observables if they are related by a gauge transformation. The group of transformations (lattice, gauge, and combined transformations) that do not modify an *Ansatz* is called the projective symmetry group (PSG). Its subgroup of pure gauge transformations is called the invariance gauge group (IGG).[3]

One may be interested in states for which all the physical quantities are invariant under the lattice symmetries. To classify these "uniform" states, one can first fix the IGG and then look for the "algebraic" PSG, which obey the constraints derived from the algebraic structure of lattice symmetry group S_L.[3] The actual *Ansätze* can then be constructed.

Clearly, there is a close correspondence between the construction of RMO's discussed in this paper and that of symmetric *Ansätze*. This correspondence is summarized in Table I.

TABLE I. Analogy between the construction of RMO's and that of symmetric *Ansätze* in Ref. 3.

	Classical spin models	Quantum mean field
State	Regular magnetic order	Physically symmetric *Ansatz*
Internal symmetry group	S_S (global spin rotation, etc.)	Φ (local gauge transformations)
Symmetry group of a state	H_c	PSG
Unbroken internal symmetries	H_c^S	IGG

[1] J. Villain, J. Phys. Fr. **38**, 385 (1977).
[2] K. Kubo and T. Momoi, Z. Phys. B **103**, 485 (1997).
[3] X.-G. Wen, Phys. Rev. B **65**, 165113 (2002).
[4] D. B. Litvin, Acta Crystallogr. A **57**, 729 (2001).
[5] F. Wang and A. Vishwanath, Phys. Rev. B **74**, 174423(2006).
[6] H. S. M. Coxeter, *Regular Polytopes*, 3rd edition (Dover, New York, 1973).
[7] B. Bernu, P. Lecheminant, C. Lhuillier, and L. Pierre, Phys. Rev. B **50**, 10048 (1994).
[8] P. Lecheminant, B. Bernu, C. Lhuillier, and L. Pierre, Phys. Rev. B **52**, 6647 (1995).
[9] J. M. Luttinger and L. Tisza, Phys. Rev. **70**, 954 (1946).
[10] M. Roger, Phys. Rev. Lett. **64**, 297 (1990).
[11] A. V. Chubukov and D. I. Golosov, J. Phys. Condens. Matter **3**, 69 (1991).
[12] J.-B. Fouet, P. Sindzingre, and C. Lhuillier, Eur. Phys. J. B **20**, 241 (2001).
[13] J. Villain, R. Bidaux, J. Carton, and R. Conte, J. Phys. Fr. **41**, 1263 (1980).
[14] E. Shender, Sov. Phys. JETP **56**, 178 (1982).
[15] C. L. Henley, Phys. Rev. Lett. **62**, 2056 (1989).
[16] A. V. Chubukov and Th. Jolicoeur, Phys. Rev. B **46**, 11137 (1992).
[17] S. E. Korshunov, Phys. Rev. B **47**, 6165 (1993).
[18] J.-C. Domenge, P. Sindzingre, C. Lhuillier, and L. Pierre, Phys. Rev. B **72**, 024433 (2005).
[19] O. Janson, J. Richter, and H. Rosner, Phys. Rev. Lett. **101**, 106403 (2008); J. Phys.: Conf. Ser. **145**, 012008 (2009).
[20] A. Lauchli, J. C. Domenge, C. Lhuillier, P. Sindzingre, and M. Troyer, Phys. Rev. Lett. **95**, 137206 (2005).
[21] A. Chubukov, E. Gagliano, and C. Balseiro, Phys. Rev. B **45**, 7889 (1992).
[22] T. Momoi, K. Kubo, and K. Niki, Phys. Rev. Lett. **79**, 2081 (1997).
[23] W. LiMing, G. Misguich, P. Sindzingre, and C. Lhuillier, Phys. Rev. B **62**, 6372 (2000).
[24] O. I. Motrunich, Phys. Rev. B **72**, 045105 (2005).
[25] T. Grover, N. Trivedi, T. Senthil, and P. A. Lee, Phys. Rev. B **81**, 245121 (2010).
[26] N. Mermin and H. Wagner, Phys. Rev. Lett. **17**, 1133 (1966).
[27] P. Chandra, P. Coleman, and A. Larkin, J. Phys. Condens. Matter **2**, 7933 (1990).
[28] C. Weber, L. Capriotti, G. Misguich, F. Becca, M. Elhajal, and F. Mila, Phys. Rev. Lett. **91**, 177202 (2003).
[29] L. Capriotti and S. Sachdev, Phys. Rev. Lett. **93**, 257206 (2004).
[30] J.-C. Domenge, C. Lhuillier, L. Messio, L. Pierre, and P. Viot, Phys. Rev. B **77**, 172413 (2008).
[31] L. Messio, Ph.D. thesis, Université Pierre et Marie Curie (2010).